Photonic Signal Processing for Phase-Agnostic Coherent Optical Reception

Bernhard Schrenk
AIT Austrian Institute of Technology, Vienna, Austria.

Abstract
Coherent optical detection has eventually brushed off its flavor of being exclusively dedicated to longhaul and metro-scale data transmission. It is now introduced to the short-reach realm, where simplicity and cost/energy-effectiveness are paramount. Towards this direction, a photonic signal processing circuit for signal recovery is introduced and experimentally evaluated in two phase-agnostic coherent receiver architectures that build on either a 90° or 120° hybrid for mixing a free-running local oscillator with a real-valued data signal. The required envelope detection function after coherent detection is accomplished through re-translating the beat signal into the optical domain, which is accomplished by leveraging highly efficient current-to-frequency conversion that enables a direct-drive scheme for the photonic signal processing circuit without extra amplification of the detected photocurrent. Squaring and summing of the quadratures is then performed in the optical domain through either an interferometric filter or a compact micro-ring resonator. It is demonstrated that the photonic outline of the signal processing chain does not necessarily go with an overhead in energy and size – but can instead be more efficient than electronics-based analogue circuitry, both in terms of power consumption and device footprint.

I. Introduction

Coherent optical detection is of high interest in the field of optical telecommunications due to its unique offerings when it comes to accessing phase information, its unprecedented sensitivity and spectral selectivity. However, these advantages come at a high degree of implementation complexity, which hinders its practical introduction in cost-sensitive segments such as intra-datacenter networks or optical access [1-3]. Various coherent transmission architectures have been investigated to strike a balance between performance gains and complexity, primarily targeting a simplification of the coherent receiver sub-system and the involved signal processing methods.

Progress in photonic integration technology has enabled recent works to demonstrate chip-scale full-field receivers incorporating phase-locked loops and carrier-phase recovery on hybrid opto-electronic circuitry [4-6]. Alternatively, self-homodyne coherent detection schemes have been investigated by taking additional fiber cores into consideration [7-10], in an attempt to shift complexity from the signal processing domain to the physical layer. This strategy can be reversed by the Kramers-Kronig receiver [11] that simplifies the detector hardware to a minimum, while instead requiring higher-bandwidth electronics and digital signal processing (DSP). Carrier-assisted differential detection [12, 13] can realize optical field recovery while mitigating the restriction to single-sideband modulated formats and the burden of a local oscillator (LO).

Further simplification concerning DSP-less reception is possible when moving from full-field reception to phase-agnostic detection of real-valued data signals. Towards this direction, earlier works have demonstrated analogue signal processing performing envelope detection in the radio frequency (RF) domain through coherent heterodyne and intradyne phase-diversity detection methodologies [14-17]. These works strive to push the bandwidth and energy efficiency of the involved RF electronics, which ultimately determine the supported data rate. The fact that coherent detection is not necessarily bound to complexity is nicely pronounced in [18], demonstrating a full-duplex coherent transceiver realized through a single laser-modulator element.

This work enters the realm of photonic signal processing (ΦSP) to accomplish all required operations to support the phase-agnostic coherent detection of real-valued optical data signals. This concept has been briefly introduced in an earlier investigation [19] that is extended through the present analysis, by experimentally demonstrating that envelope detection can be conducted optically after phase-diversity reception takes place with either a 90° or 120° hybrid used as optical mixer. An efficient translation of the detected photocurrents to the optical domain is introduced, which enables a simplification of the RF domain by omitting electrical amplification and signal conditioning, thus opening avenues for a highly energy efficient and compact implementation of the signal processing stage. Towards this, it will be shown that the ΦSP approach outperforms RF-based analogue signal processing with regards to the reception sensitivity, the required energy consumption and the footprint of the involved circuits.

This manuscript is organized as follows. Section II introduces the concept of ΦSP and compares it to the

traditional analogue RF-based method employed for phase-agnostic coherent detection. Section III introduces the experimental framework that has been used to evaluate the proposed concept. Section IV then discusses the transmission performance for both, ΦSP and RF-based signal processing. A comparison of implementation requirements in terms of energy consumption and device footprint is made in Section V, before Section VI concludes the work.

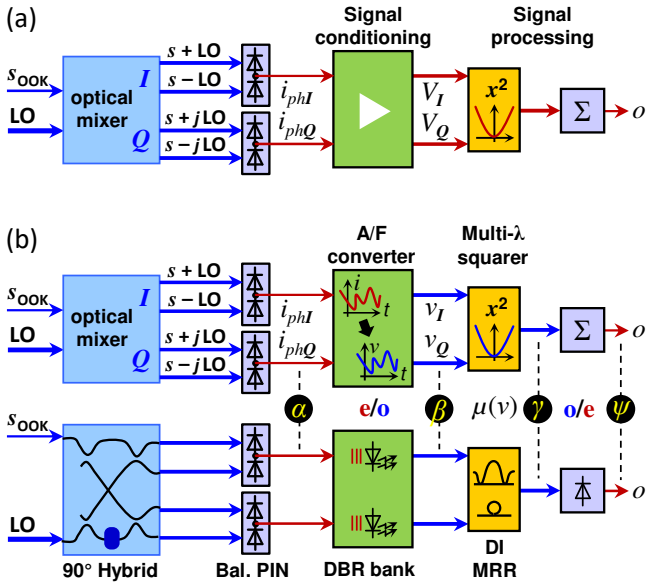

Fig. 1. (a) Conceptual scheme for phase-agnostic coherent reception and (b) related ΦSP principle with (c) corresponding implementation example.

II. Photonic Signal Processing Architecture for Phase-Agnostic Coherent Reception

Phase-agnostic coherent reception of a real-valued signal can be accomplished through phase-diversity reception [20]. Figure 1(a) introduces a representative example of a corresponding receiver with an architecture that builds on a 90° hybrid as optical mixer, whose balanced photodiodes yield the photocurrents

$$\begin{aligned} i_{\mathrm{ph}I}(t) &\propto \sqrt{P_{LO}\, s_{\mathrm{OOK}}(t)}\cos\left(\Omega_{\mathrm{IF}}t+\varphi(t)\right), \\ i_{\mathrm{ph}Q}(t) &\propto \sqrt{P_{LO}\, s_{\mathrm{OOK}}(t)}\sin\left(\Omega_{\mathrm{IF}}t+\varphi(t)\right) \end{aligned} \qquad (1)$$

for the I and Q quadratures, respectively. Here, s_{OOK} stands for the transmitted on-off keyed (OOK) data signal, P_{LO} for the power of the LO, Ω_{IF} denotes the intermediate frequency (IF) that results from coherent intradyne detection with a free-running LO, and φ accounts for the corresponding phase noise. To recover the original data signal s_{OOK}, envelope detection can be performed according to

$$o(t) = i_{\mathrm{ph}I}{}^2(t) + i_{\mathrm{ph}Q}{}^2(t) \qquad (2)$$

which resembles the transmitted OOK data. Such a processing function has been demonstrated in the analogue RF domain through use of signal conditioning followed by four-quadrant multiplication.

The present investigation instead focuses on signal processing in the analogue optical domain, as it has been recently introduced for the purpose of duobinary demodulation or multi-level symbol slicing [21]. For the purpose of envelope detection, the ΦSP is employed according to the constituent functions that are detailed in Fig. 1(b). The ΦSP commences with a conversion of the I and Q photocurrents of the coherent receiver back to the optical domain. This is accomplished by an amplitude-to-frequency (A/F) converter that is directly fed by the balanced PIN photodiodes, without extra signal conditioning such as contributed through electrical amplification. The frequency-domain representations are then squared in the optical domain and the sum of squares, according to Eq. (2), completes the signal processing during the subsequent photodetection. In the following, the constituent functions that collectively serve the ΦSP chain are discussed in detail.

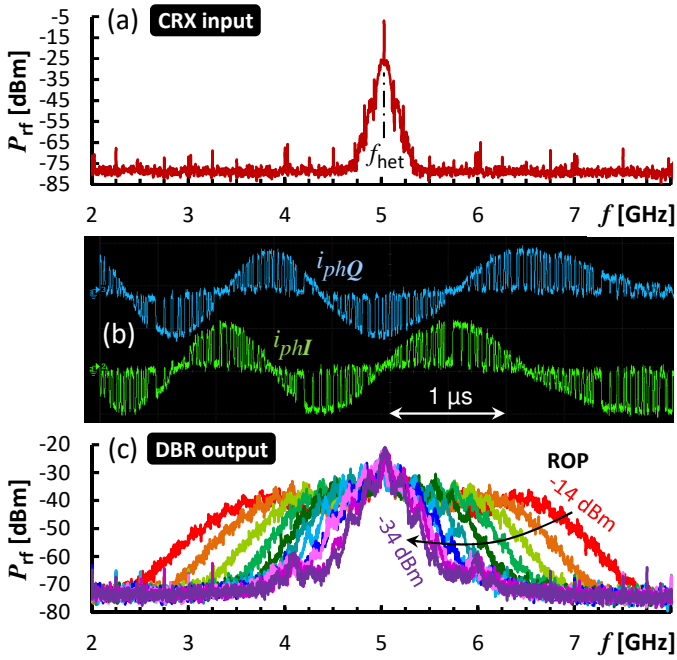

Fig. 2. (a) Heterodyned RF spectrum for CRX input OOK signal at an IF much larger than the symbol rate. (b) *I*,*Q* photocurrents after intradyne coherent reception, with an IF much smaller than the symbol rate. (c) Heterodyned DBR output spectrum as a function of the ROP.

A. Direct-Drive A/F Converter

A laser with modulated distributed Bragg reflector (DBR) is employed as an efficient optical frequency modulator. The DBR section of the laser is directly driven by the unamplified photocurrent $i_{ph}(t)$. With this, the optical emission frequency v of the laser, which can be typically tuned by several nanometers, is not only coarsely determined by its bias current, but finely adjusted by the additional DBR drive current. Provided that the induced modulation remains within a DBR laser mode, the instantaneous optical frequency of the frequency modulated (FM) signal becomes

$$v = v_0 + v_\Delta \cdot i_{ph}(t), \qquad (3)$$

with v_0 being the nominal emission frequency of the DBR laser at its bias point and v_Δ denotes its conversion efficiency for translating a drive current into a frequency excursion.

Figure 2 gives an example about the FM efficiency that is characteristic for a DBR laser that will be later used in the experiment: The input data signal to the coherent receiver in Fig. 1(b), presented in Fig. 2(a) in terms of an RF spectrum after heterodyning it with a reference laser to an IF at $f_{het} \approx 5$ GHz, features a low bandwidth of 100 MHz. Figure 2(b) reports the *I* and *Q* time-domain photocurrents that are generated by this data signal at a received optical power (ROP) of -20 dBm after coherent phase-diversity reception. A peak-to-peak current of ~150 μA_{pp} is yielded for a LO power of 9 dBm to the optical 90° mixer, taking typical excess losses for the optical hybrid and polarization controller into consideration. When using these photocurrents to directly drive a DBR laser, the (again heterodyned) DBR output signal of Fig. 2(c) is obtained. This output is presented for a step size of 2 dB in the ROP range from -14 to -34 dBm to the coherent receiver (CRX). As can be noticed, there is a high contrast between the original input data signal bandwidth (Fig. 2(a)) and the much wider frequency deviation of more than 3 GHz for the DBR output – despite the unamplified DBR drive. This renders the DBR laser as a highly efficient A/F converter but also requires the subsequent photoreceiver to provision an opto-electronic bandwidth wider than the transmitted data bandwidth. Nonetheless, broadband PIN photodiodes are typically available in mature photonic integration platforms.

B. Optical Sum of Squares

With the *I* and *Q* quadratures of the coherent receiver now being represented by their frequency-domain representations, the process of squaring becomes a simpler exercise since it can be accomplished with suitable optical filters. The investigation in this work will focus on two filter types, including an asymmetric Mach-Zehnder delay interferometer (DI) and a micro-ring resonator (MRR). Provided that these filters have a periodic transfer function, the squaring process can be further accommodated for multiple wavelength channels, essentially meaning that only one filter is required for square both quadratures.

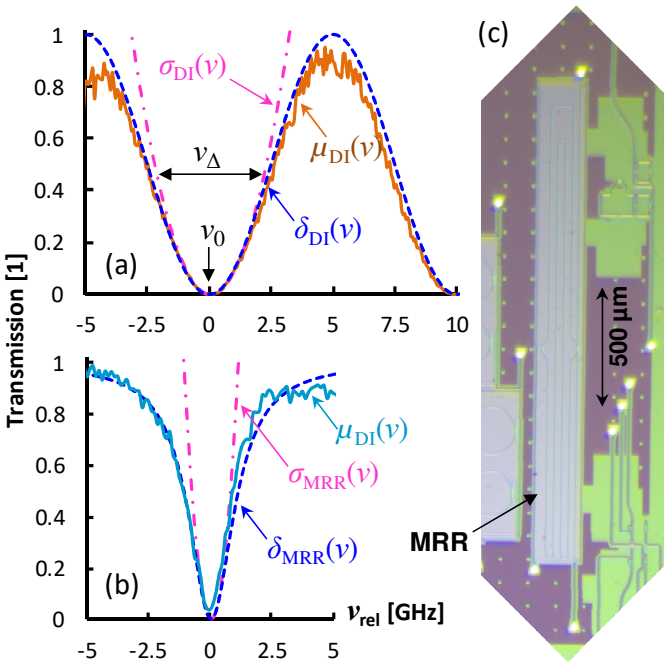

Fig. 3. (a) Transfer function δ, measured response μ and approximation as square function σ for (a) the DI and (b) the MRR, for which (c) shows a chip photograph.

Figure 3(a) presents the measured optical transfer function $\mu_{DI}(v)$ of a 10-GHz DI that will be employed as the multi-wavelength squarer in the further experimental assessment. The periodic transmission of the DI is shown as function of the relative optical frequency v to one of its notches. Further included is the theoretical transmission function

$$\delta_{DI}(v) = ½ [1 - cos(2\pi v\ \Delta T)] \qquad (4)$$

where ΔT stands for the differential delay introduced by the longer arm of the DI. This differential delay corresponds to the inverse of the free spectral range (FSR). If $\delta_{DI}(v)$ is observed close to its spectral notch, where $|v| < FSR/4$, there is a good overlap with the approximation function

$$\sigma_{DI}(v) = (\pi v\ \Delta T)^2. \qquad (5)$$

This means that a square-function is obtained at the notch of the DI. The carrier offset v_0 is then chosen to spectrally center the frequency-domain representations of the photocurrents to any of the DI notches yielded by its periodic transfer function. The frequency deviation v_Δ of the FM photocurrents is kept small enough to remain in the quadratic region of the DI transfer function, close to its notch frequencies. Given that the power levels of the two FM input signals are balanced, the output signal of the DI, which is detected by a photoreceiver, then becomes

$$o_{DI}(t) \sim \sum[\pi v\ i_{phI,Q}(t) / FSR]^2. \qquad (6)$$

This result corresponds to the desired signal processing function sought for phase-agnostic coherent detection. In case the two inputs of the DI are imbalanced in their transmission function, the signal processing stage requires an initial calibration that balances the I, Q path losses through choosing the DBR launch for each branch accordingly. The DI used for the experimental evaluation showed a loss imbalance of 0.14 dB for its two ports.

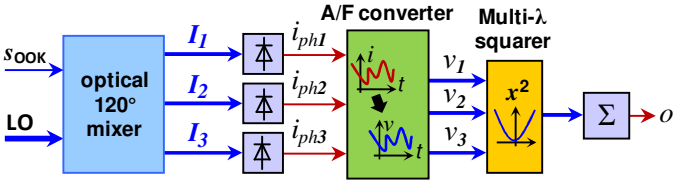

Fig. 4. ΦSP principle adopted for a phase-diversity CRX based on a 120° hybrid as optical mixer.

The DI-based multi-wavelength squarer, which necessitates a large device footprint to implement its delay ΔT, can be substituted by a more compact MRR. Figure 3(b) presents the transfer characteristics of this alternative filter implementation. The measured transfer function $\mu_{\mathrm{MRR}}(\nu)$ has been acquired for the silicon MRR that is shown in Fig. 3(c). The MRR has been fabricated on silicon-on-insulator (SoI) technology with a 220×500 nm^2 waveguide cross-section. Its FSR is 9.3 GHz and the FWHM bandwidth for the drop transmission is 1.6 GHz. The footprint of the folded MRR structure is 220×2050 μm^2. Figure 3(b) further includes the theoretical transmission function [22] for the through-port of a MRR,

$$\delta_{MRR}(\nu) = 1 - \frac{1}{1 + \frac{4F^2}{\pi^2}\sin^2\left(\frac{2\pi^2 r_{MRR} n_{eff} \nu}{c_0}\right)} \tag{7}$$

where F stands for the finesse, r_{MRR} denotes the equivalent radius of an unfolded MRR structure, n_{eff} is the effective refractive index, and c_0 the speed of light. This transmission function can be approximated by

$$\delta_{MRR}(\nu) = \frac{\xi \nu^2}{1 + \xi \nu^2} \tag{8}$$

where

$$\xi = \left(\frac{2F\, r_{MRR} n_{eff}}{c_0}\right)^2 \tag{9}$$

At the resonance frequency of the MRR, this transmission function can be further approximated by the square function

$$\sigma_{MRR}(\nu) \sim \xi \nu^2 \tag{10}$$

The desired output $o(t)$ of the recovered data signal is then obtained by centering the frequency-domain representations of the I and Q quadratures at the spectral notches of the MRR while leveling their frequency deviation.

To compare the proposed ΦSP scheme to alternative CRX implementations, Figure 4 presents a as a phase-agnostic and, at the same time, simplified receiver implementation based on a 120° hybrid. The corresponding photocurrents $i_{ph1\ldots3}$ of this receiver with a reduced number of photodiodes now show a 2π/3 phase shift for their IF when a 3×3 coupler is used as optical mixer, as elaborated in detail in [23]. The original data signal can be similarly yielded by again producing the sum of squares of the photocurrents [14]. Section IV.B will evaluate this simplified receiver configuration when adopting the proposed ΦSP concept.

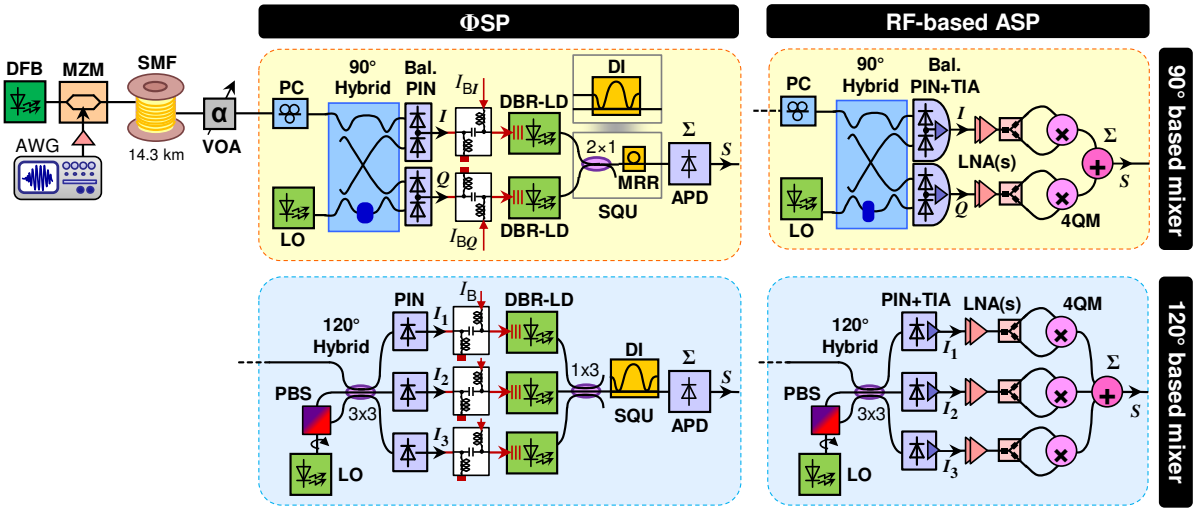

Fig. 5. Experimental setup with the CRX implementations for ΦSP and RF-based ASP with optical 90° and 120° mixers.

III. Experimental Evaluation

The proposed ΦSP technique and traditional RF-based analogue signal processing (ASP) have been evaluated using the setup shown in Fig. 5. An OOK signal was modulated on an optical carrier at 1550 nm using an arbitrary waveform generator (AWG) that drives a Mach-Zehnder modulator (MZM). The signal was then transmitted over a standard single-mode fiber (SMF) span with a length of 14.3 km and a variable optical attenuator (VOA) set the ROP to a coherent phase-diversity receiver that builds on either a 90° or a 120° hybrid as optical mixer between the signal and a LO. The free-running LO had an optical power of 9 dBm and was tuned to the optical input signal so to minimize the frequency offset, resulting in an intradyne detection scenario. The input state of polarization to the optical mixer has been controlled using a manual polarization controller (PC). In this way, the performances between ΦSP and ASP can be accurately compared, without further influence by a random input polarization state. Nonetheless, polarization diversity or multiplexing can be supported through modification of the coherent receiver architecture, as for example demonstrated in [4, 6, 9, 14, 16, 24].

The electrical back-end following the photodetection at the output of the optical mixer differs between both signal processing architectures: For the RF-assisted ASP-based scheme based on 90° hybrid, the balanced PIN detectors are co-integrated with transimpedance amplifiers (TIA) characterized by a transimpedance of Z_T = 60 dBΩ. The detected signals are further conditioned by low-noise amplifiers (LNA) with a gain of 10 dB/stage, to pre-compensate for the loss of the subsequent four-quadrant RF multipliers (4QM) that serve the envelope detection of the *I*,*Q* quadratures.

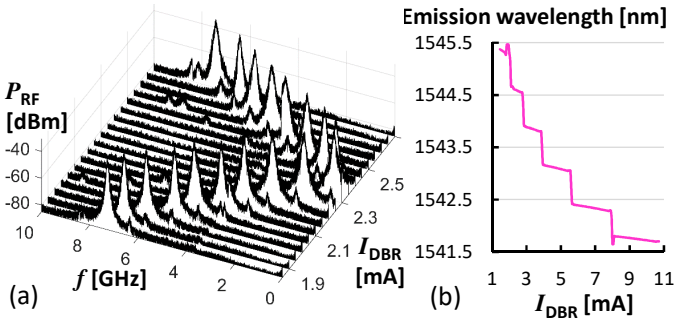

Fig. 6. DBR laser tuning: (a) heterodyned beat note and (b) emission wavelength as a function of the DBR current.

For the alternative ΦSP scheme the raw photocurrents of the balanced PIN diodes are directly driving the DBR sections of the respective lasers used for A/F conversion – without employing TIA or LNA stages for the purpose of signal conditioning. The gain section of the DBR laser was biased at 40 mA, yielding an output power of 1.4 dBm. The bias points of the balanced photodiodes and the DBR lasers in the *I* and *Q* branches of the coherent receiver are independently chosen through a cascade of bias-Ts. With this, dedicated bias points I_{BI} and I_{BQ} can be defined for the DBR lasers, resulting in different optical frequencies ν_0 for the FM representations of the photocurrents. The optical frequencies at the laser outputs tune with 17.9 GHz/mA, owing to the wide tunability of their DBR sections (Fig. 6). Consequently, different spectral notches can be selected for the multi-wavelength squarer (SQU) and a sum function can be accomplished without signal-signal interference. The SQU was either chosen to be the aforementioned 10-GHz DI, for which the *I* and *Q* quadratures can be launched into its complementary ports, or the silicon MRR that is preceded by a colorless 50/50 coupler to simultaneously use the through-port of the MRR for both quadratures. A photoreceiver with TIA back-end then converts the sum of squared *I* and *Q* quadratures to the electrical domain. An avalanche photodetector (APD) was chosen as opto-electronic summing element to accommodate the fiber-to-fiber pass-through loss of ~16 dB when squaring the FM signals with the SoI-based MRR. The signal was then digitized with a real-time scope and the bit error ratio (BER) has been estimated to serve the performance comparison.

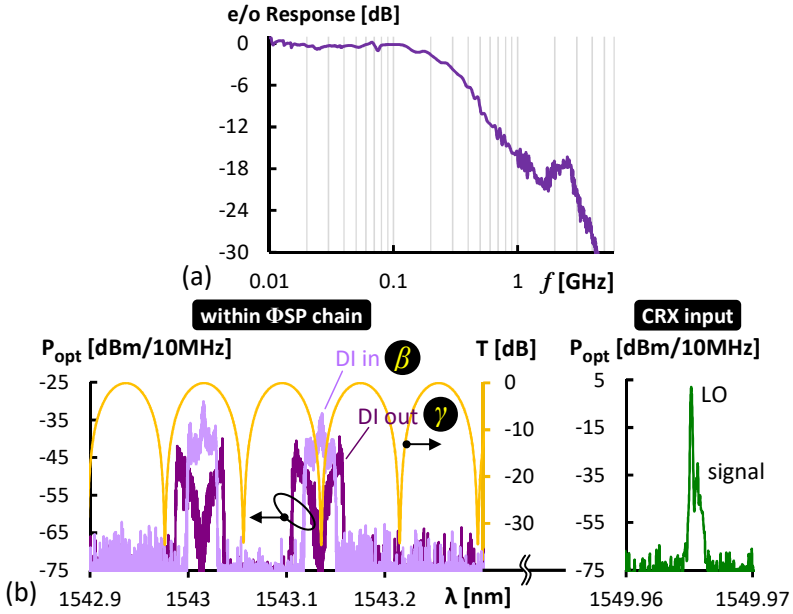

Fig. 7. (a) Electro-optic modulation bandwidth of the DBR section. (b) Optical spectra at the CRX input and for the resulting frequency-translated *I*,*Q* photocurrents before and after spectral processing through the DI.

Even though the DBR lasers show an exceptional efficiency as an A/F converter, their electro-optic response for DBR modulation drops sharply after reaching its 3dB-bandwidth of 270 MHz (Fig. 7(a)). This is presently seen as the main limitation for the presented experiment, as it limits the symbol rate of the OOK data signal to R_{sym} = 100 Mb/s to remain in the flat region of the electro-optic response. However, DBR lasers with a much faster DBR response of up to 10 GHz have been demonstrated elsewhere [25], while further potential for a fast A/F conversion is provided through various fast tunable laser implementations [26-28].

Figure 5 further presents the experimental configurations for the CRX based on a 120° hybrid as optical mixer. These CRX follow a layout in tight analogy to the earlier discussed implementations, with the difference that polarization-insensitive reception is obtained by applying a diversity LO feed to the 3×3 coupler serving as optical mixer [14].

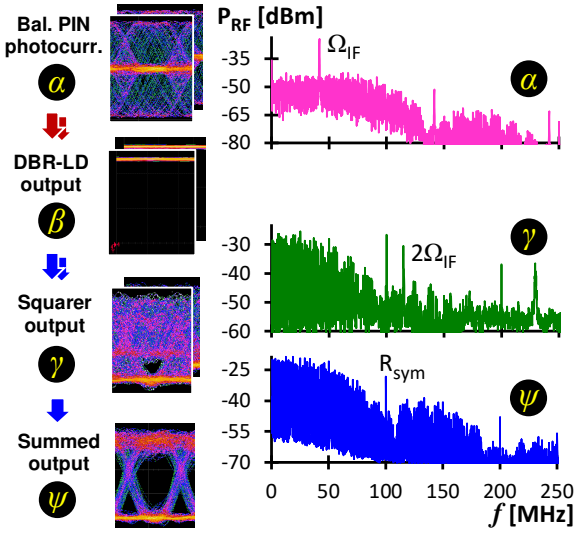

Fig. 8. Eye diagrams along the ΦSP chain and corresponding RF signal spectra.

IV. Signal Recovery Performance

A. Phase-diversity CRX based on 90° optical mixer

Figure 7(b) reports the optical spectra at the CRX input, where the LO beats with the OOK signal, and within the ΦSP unit at the in- and output of the DI, respectively. The FM-translated versions (β) of the *I* and *Q* photocurrents of Fig. 2(b) are aligned in a way that they oscillate around the spectral notches of the

complementary DI ports, for which the transmission T is appended to Fig. 7(b). The peak-to-peak swing of ~150 µA for the photocurrents at a ROP of -20 dBm is large enough to accommodate a frequency deviation v_Δ that pairs well with the FSR of the DI. The output spectrum of the DI (γ) shows the squaring function as it is indicated by the wider spectral signal bandwidth.

Figure 8 presents the corresponding RF signal spectra. Shown are the photocurrent after coherent detection (α) with its IF at $\Omega_{IF} < R_{sym}$ that results from the detuning between the LO and the input data signal and the squared I signal (γ) with a signature at $2\Omega_{IF}$. This signature in γ is slightly offset from the value Ω_{IF} of the photocurrent in α, which is a result of the different acquisition times and the limited longer-term stability of the LO and signal lasers. Further reported is the sum of squares (ψ), for which the suppression of either Ω_{IF} or $2\Omega_{IF}$ proves the correct operation of the ΦSP chain that recovers the original data signal with symbol rate R_{sym}. This is evidenced by the eye diagrams, which have been appended to Fig. 8. The suppression of $2\Omega_{IF}$ can be used as a performance indicator to align the input signals to the spectral notch of the rectifier during the initial spectral setup or to compensate for possible long-term drifts of the optical squarer against the DBR lasers.

The BER performance for the CRX with 90° hybrid as optical mixer is presented in Fig. 9. Results are shown for applying photonic (solid lines) and RF-based analogue (dashed lines) signal processing. The performance has been evaluated for various signal conditioning layouts after photodetection. In case of the most simplified receiver layout, where the balanced photodiodes directly drive the DBR lasers without additional RF amplification, the ΦSP circuit obtains a sensitivity of -30.1 dBm at a BER of 10^{-3} when using the DI as optical squarer (▲). The remarkable signal integrity is evidenced by the clear eye diagram appended to Fig. 9. If the DI is substituted by the more compact MRR, the sensitivity improves by 2.1 dB (◆). This improvement is attributed to the smaller bandwidth of the MRR notch, as it has been reported in Fig. 3(b). This permits the use of a lower DBR drive, which beneficially translates to a lower ROP. There was no penalty incurred for transmission over 14.3 km of SMF (■). Moreover, RF-based ASP cannot obtain a BER below 5.8×10^{-2} under the direct-drive condition for its signal processing stage, even when raising the ROP to 3 dBm (see corresponding eye in Fig. 9).

When signal amplification for the raw photocurrents is additionally adopted after photodetection, the reception sensitivities improve further. For PIN+TIA based balanced photoreceivers that now drive the DBR lasers with an amplified photocurrent, the reception sensitivity enhances to -55.7 dBm (●) by virtue of the transimpedance gain. This vast improvement nevertheless comes at the expense of adding RF circuitry to a previously purely opto-electronic receiver layout, which could be entirely realized on a photonic integrated circuit. The alternative RF-based ASP approach accomplishes a BER of 10^{-3} for a ROP of -39.7 dBm (×). It cannot reach the sensitivity with the ΦSP receiver, even after adding one (+) or two (○) more LNAs to address the driving requirement of the RF-based four-quadrant multiplier.

For the sake of completeness the ΦSP configuration with single-ended PIN detectors at the I,Q outputs of the 90° hybrid has been included in Fig. 9 (△) for the case of not using a TIA for conditioning of the photocurrents. Here, a sensitivity of -23.1 dBm is obtained at a BER of 10^{-3}, which relates to a penalty of 7 dB with respect to a balanced photodetector. The penalty is directly related to the reduced swing of the photocurrent generated by the single-ended detector configuration, which according to Eq. (1) needs to be offset by a higher ROP.

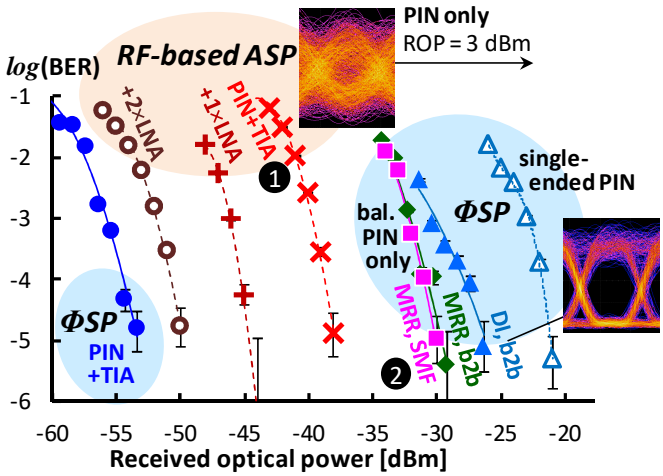

Fig. 9. BER performance for ΦSP and RF-based ASP for a CRX based on a 90° hybrid as optical mixer.

B. Phase-diversity CRX based on 120° optical mixer

Figure 10 reports the BER performance for the CRX with 120° mixer and single-ended photodiodes. The sensitivities are clearly worse than for the CRX that builds on a 90° mixer and balanced photodiodes, herein referred to as the reference receiver. This penalty applies to both, the ΦSP (▲,●) and the RF-based ASP (+,○).

For the direct-drive ΦSP scenario without TIA, a sensitivity of -25.7 dBm (▲) is obtained, which relates to a penalty of 4.4 dB with respect to the reference receiver evaluated in Section IV.A. This penalty is attributed to the natural reduction in DBR drive that comes when using a single-ended rather than a balanced photodetector. When employing a TIA, the sensitivity again improves vastly to -46.8 dBm (●), however, the penalty rises to 8.9 dB. This is not only a result of the reduced RF photocurrent swing available to feed the ΦSP chain, but also derives from a 2-dB reduction of LO power that was necessary to maintain linear TIA operation without being affected by a saturation onset due to a high DC photocurrent arising from the unbalanced photodetector configuration.

In case of RF-based ASP, sensitivities between the direct-drive and amplified ΦSP scenarios are obtained when one (+) or two LNAs (○) are following the photodetector as signal conditioning elements. The relative BER performance towards the ΦSP resembles the findings for the CRX based on 90° mixer.

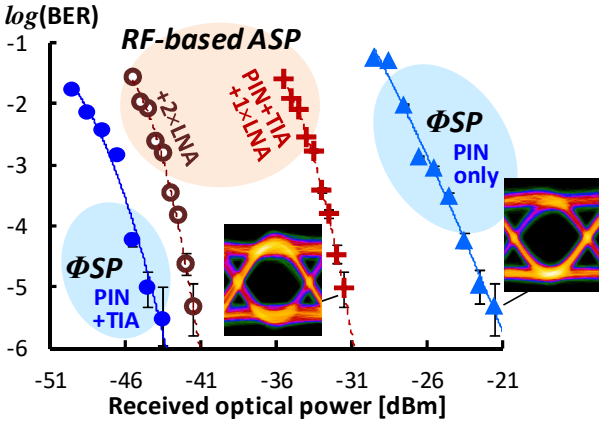

Fig. 10. BER performance for ΦSP and RF-based ASP for a CRX based on a 120° hybrid as optical mixer.

V. Energy Consumption and Required Circuit Footprint

Given the reception performance in Section IV.A, the energy consumption and the required device footprint can be compared among ΦSP- and RF-based signal processing methods. This comparison has been conducted for the CRX architecture based on 90° hybrid and is summarized in Table I.

The RF-based ASP employs two commercial four-quadrant multipliers (AD834) that are driven by the balanced PIN+TIA receivers (based on the OPA847 model) without further LNAs (× in Fig. 9). A micro-Peltier element integrated with the LO is assumed, which also applies for the ΦSP circuit. This temperature control shall be a common feature of the entire electro-optic CRX package so that it is excluded from the specific footprint estimation.

The ΦSP method, on the other hand, differs through its ability to recover the signal with a direct drive of its photonic circuitry through the raw photocurrents. The photonic circuit can capitalize on the efficient amplitude-to-frequency conversion through DBR lasers, which is compatible with the direct photocurrent drive (few tens of μA_{pp}) by the balanced PIN photodiodes. Therefore, no TIA is required for the balanced photodetectors. This considerably reduces the energy consumption. However, this advantage is offset by the need for two DBR lasers, whose gain sections are primarily responsible for the overall power consumption. Moreover, an extra photodetector with TIA back-end is required when converting the processed ΦSP output back to the electrical domain. No spectral tuning has to be accounted for the optical squarer, for which the MRR has been considered (◆ in Fig. 9). This is due to the fact that simple tunable lasers are already employed as light source, mitigating the need for an energy-hungry thermo-optic tuning of the squarer. The MRR can be implemented on a rather compact space, as detailed in Section II. Similarly, earlier works have shown a feature size of 620 μm^2 when implementing a 90° hybrid as optical mixer [29]. Moreover, lasers and photodetectors are available as integrated waveguide devices and feature a much smaller footprint than RF circuits, for which a space of 0.79 and 1.88 mm^2 apply for TIA and 4QM, respectively.

The contributions over the entire signal processing chains eventually lead to an overall improvement when adopting the ΦSP scheme. These improvements amount to 3.3 and 6.1 dB in terms of energy consumption and circuit footprint, respectively. This clearly underpins the beneficial aspects of the ΦSP concept.

The efficiency of the ΦSP circuit is further pronounced when comparing the two CRX architectures. Given the BER performances, the MMR-based ΦSP circuit for the CRX with 90° mixer and TIA-less balanced photodetectors (■ in Fig. 9) performs as good as the RF-based ASP for the CRX with 120° mixer and single-ended PIN+TIA with one additional LNA (+ in Fig. 10). An omission of TIA and LNA circuits can be therefore

accomplished through the rather trivial inclusion of one additional photodiode, without penalty in reception performance.

Table I
Energy consumption and footprint for photonic and RF-based signal processing.

Element \ Processing			❶ Analog RF		❷ Photonic	
			mW	mm^2	mW	mm^2
CRX	LO	1×	84	0.025	84	0.025
	90° hybrid	1×	–	6.10^{-4}	–	6.10^{-4}
	balanced PIN	2×	24	2.10^{-3}	24	2.10^{-3}
	TIA	2×	360	1.58	direct drive	
ASP	LNA	0×	0	0		
	4Q Multiplier	2×	312	3.75		
PSP	LD gain +	2×			84	0.035
	DBR	2×			6	5.10^{-3}
	MRR	1×			–	0.451
	APD+TIA	1×			77	0.789
com	micro-TEC	1×	160	shared	160	shared
Total			940	5.36	435	1.31

VI. Conclusion

A photonic processing circuit that is dedicated to the signal recovery after phase-agnostic coherent detection has been experimentally demonstrated for two CRX architectures, involving efficient electro-optic frequency modulation, simultaneous optical squaring of multiple wavelength channels and their subsequent summation. The proposed ΦSP chain does not require RF circuits apart from bias-Ts that are solely employed to define the bias points of the constituent opto-electronic elements. Through the omission of the TIA at the CRX front-end, the involved direct-drive scheme for AM-to-FM conversion can greatly simplify the overall CRX design in links with low optical budget, boosting the energy efficiency and compressing the CRX footprint – as demonstrated in direct comparison to an analogue RF-based signal processing circuit. Scaling up the data symbol rate through DBR lasers with higher electro-optic modulation bandwidth and the implementation of more complex coherent signal processing functions are left for future work.

VII. Acknowledgement

This work was supported in part by the European Research Council (ERC) under the European Union's Horizon 2020 research and innovation programme (grant agreement No 804769).

VIII. References

[1] J. Krause Perin, A. Shastri, and J. M. Kahn, "Coherent Data Center Links", *J. Lightwave Technol.*, vol. 39, no. 3, pp. 730-741, Feb. 2021.
[2] Y. Zhu *et al.*, "Comparative study of cost-effective coherent and direct detection schemes for 100 Gb/s/λ PON," *J. Opt. Comm. Netw.*, vol. 12, no. 9, pp. 36-47, 2020.
[3] J. Zhou *et al.*, "Flexible Coherent Optical Access: Architectures, Algorithms, and Demonstrations," *J. Lightwave Technol.*, vol. 42, no. 4, pp. 1193-1202, 2024.
[4] A. Maharry *et al.*, "First Demonstration of an O-Band Coherent Link for Intra-Data Center Applications," *J. Lightwave Technol.*, vol. 41, no. 21, pp. 6643-6650, 2023.
[5] S. Chung, R. Ashok, P. Jain, S. Naaz, A. Sidhique, and S. Gupta, "An Analog EIC-PIC Receiver With Carrier Phase Recovery for Self-Homodyne Coherent DCIs," *IEEE Trans. Circ. and Sys. II: Expr. Briefs*, vol. 70, no. 2, pp. 446-450, Feb. 2023.
[6] T. Hirokawa *et al.*, "Analog Coherent Detection for Energy Efficient Intra-Data Center Links at 200 Gbps Per Wavelength," *J. Lightwave Technol.*, vol. 39, no. 2, pp. 520-531, 2021.
[7] X. Liang *et al.*, "Study of Self-Homodyne Coherent System Using Multicore Fiber for Data Center Links," *IEEE Phot. J.*, vol. 14, no. 4, art. no. 7234306, Aug. 2022.
[8] H. Du *et al.*, "Self-homodyne Coherent Detection Transmission through a (1+8) Multicore Fiber with One Polarization-maintaining Core," *J. Lightwave Technol.*, vol. 42, no. 5, pp. 1460-1468, Oct. 2023.
[9] R. Zhang, K. Kuzmin, Y.W. Chen, and W.I. Way, "800G/λ Self-Homodyne Coherent Links With Simplified DSP for Next-Generation Intra-Data Centers," *J. Lightwave Technol.*, vol. 41, no. 4, pp. 1216-1222, 2023.
[10] H. Ji *et al.*, "Photonic Integrated Self-Coherent Homodyne Receiver Without Optical Polarization Control for Polarization-Multiplexing Short-Reach Optical Interconnect," *J. Lightwave Technol.*, vol. 41, no. 3, pp. 911-918, 2023.
[11] T. Bo, and H. Kim, "Toward Practical Kramers-Kronig Receiver: Resampling, Performance, and Implementation," *J. Lightwave Technol.*, vol. 37, no. 2, pp. 461-469, Jan. 2019.
[12] W. Shieh, C. Sun, and H. Ji, "Carrier-assisted differential detection." *Light: Science & Applications*, vol. 9, no. 1, art. no. 18, 2020.

[13] J. Li *et al.*, "High electrical spectral efficiency silicon photonic receiver with carrier-assisted differential detection," in *Proc. Opt. Fiber Comm. Conf. (OFC)*, San Diego, Mar. 2022, paper Th4B.6.
[14] E. Ciaramella, "Assessment of a Polarization-Independent DSP-Free Coherent Receiver for Intensity-Modulated Signals", *J. Lightwave Technol.*, vol. 38, no. 3, pp. 676-683, Feb. 2020.
[15] J. Zhou *et al.*, "Unequally spaced PAM-4 signaling enabled sensitivity enhancement of a simplified coherent receiver applied in a UDWDM-PON," *Opt. Expr.*, vol. 30, no. 20, pp. 35369-35380, 2022.
[16] G. Silva Valdecasa, O. Gallardo Puertas, J.A. Altabas, M. Squartecchia, J. B. Jensen, and T. K. Johansen, "High-Speed SiGe BiCMOS Detector Enabling a 28 Gbps Quasi-Coherent Optical Receiver," *IEEE Trans. Circ. and Sys. II: Expr. Briefs*, vol. 69, no. 3, pp. 964-968, Mar. 2022.
[17] N. Nambath, R.K. Raveendranath, D. Banerjee, A. Sharma, A. Sankar, and S. Gupta, "Analog Domain Signal Processing-Based Low-Power 100-Gb/s DP-QPSK Receiver," *J. Lightwave Technol.*, vol. 33, no. 15, pp. 3189-3197, 2015.
[18] B. Schrenk, "The Electroabsorption-Modulated Laser as Optical Transmitter and Receiver: Status and Opportunities", *IET Optoelectronics*, vol. 14, no. 6, pp. 374-385, Dec. 2020.
[19] B. Schrenk, "Energy / Footprint Efficient Photonic Signal Processing of Raw Photocurrents in Phase-Agnostic Coherent Receiver," in *Proc. Europ. Conf. Opt. Comm. (ECOC)*, Sep. 2024, Frankfurt, Germany, paper W2A.67.
[20] A. Davis, M. Pettitt, J. King, and S. Wright, "Phase Diversity Techniques for Coherent Optical Receivers," *J. Lightwave Technol.*, vol. 5, no. 4, pp. 561-572, Apr. 1987.
[21] B. Schrenk, and M. Stephanie, "ΦPU – A Photonic Processing Unit for Heterogeneous Optical Networks", *J. Lightwave Technol.*, vol. 42, no. 22, pp. 7989-7998, Nov. 2024.
[22] A. Ayazi, T. Baehr-Jones, Y. Liu, A. E. J. Lim, and M. Hochberg, "Linearity of silicon ring modulators for analog optical links," *Opt. Expr.*, vol. 20, no. 12, pp. 13115-13122, May 2012.
[23] C. Xie *et al.*, "Colorless coherent receiver using 3x3 coupler hybrids and single-ended detection," *Opt. Expr.*, vol. 20, no. 2, pp. 1164-1171, Jan. 2012.
[24] B. Schrenk, and F. Karinou, "Simple Laser Transmitter Pair as Polarization-Independent Coherent Homodyne Detector," *Opt. Expr.*, vol. 27, no. 10, pp. 13942-13950, May 2019.
[25] M. Pantouvaki, C.C. Renaud, P. Cannard, M.J. Robertson, R. Gwilliam, and A.J. Seeds, "Fast Tuneable InGaAsP DBR Laser Using Quantum-Confined Stark-Effect-Induced Refractive Index Change," *J. Sel. Topics in Quantum Electron.*, vol. 13, no. 5, pp. 1112-1121, Sep. 2007.
[26] J.M. Fabrega *et al.*, "Modulated Grating Y-Structure Tunable Laser for λ-Routed Networks and Optical Access," *J. Sel. Topics in Quantum Electron.*, vol. 17, no. 6, pp. 1542-1551, Nov. 2011.
[27] Y. Ueda, T. Shindo, S. Kanazawa, N. Fujiwara, and M. Ishikawa, "Electro-optically tunable laser with ultra-low tuning power dissipation and nanosecond-order wavelength switching for coherent networks," *Optica*, vol. 7, no. 8, pp. 1003-1006, Aug. 2020.
[28] S. Dhoore, G. Roelkens, and G. Morthier, "Fast Wavelength-Tunable Lasers on Silicon," *J. Sel. Topics in Quantum Electron.*, vol. 25, no. 6, art. no. 1500908, Nov. 2019.
[29] H. Guan *et al.*, "Compact and low loss 90° optical hybrid on a silicon-on-insulator platform," *Opt. Expr.*, vol. 25, no. 23, pp. 28957-28968, Nov. 2017.